Performance Analysis of Hybrid Optimized Pi Controller For Sepic Converter Based Grid Tied Electric Vehicle

K.S.KAVIN[1], P. SUBHA KARUVELAM[2] AND M. GNANA SUNDARI[3],

Research Scholar[1], Professor[2,3]

Department of EEE, Government College of Engineering, Tirunelveli, 627007, Tamilnadu, India

**Corresponding Author: K.S.Kavin. Email: kavinksk@gmail.com*

ABSTRACT

The Electric Vehicles (EVs) are garnering immense attention in recent times, since they support sustainable transportation with minimized carbon emission. The amount of carbon footprint released to the atmosphere is further reduced with the adoption of Photovoltaic (PV) based EVs. The PV output is initially fed to a DC-DC SEPIC converter, which produces high dc voltage with non-inverting output and reduced switching loss. The operation of the SEPIC converter is controlled using a Hybrid Grey Wolf Optimization (GWO)-Particle Swarm Optimization (PSO) based Proportional Integral (PI) controller for providing a stable DC voltage to the three phase Voltage Source Inverter (3φ VSI). The 3φ VSI output is used to power the BLDC motor of the EV. The power from the PV is sufficient for the EV application during daytime, however, during night time with the absence of the sun, the BLDC motor is supplied with the power from the grid. The grid is connected to this system through a Single Phase (1φ) VSI. The proposed control method is verified using MATLAB simulation and the hybrid GWO-PSO algorithm delivers an outstanding efficiency of 96%.

Keywords: *PV system, SEPIC converter, Hybrid GWO-PSO Optimized PI controller, BLDC motor*

INTRODUCTION

The growing concerns regarding the negative impacts of Global warming along with climate change has necessitated the development of an effective transportation and energy generation system with lower carbon footprint. The fossil fuel-based vehicles and energy generation system are the major contributors of harmful carbon emissions in our atmosphere. Therefore, the adoption of PV based EVs is instrumental in providing an effective solution to tackle climate change. The EVs are eco-friendly mode of transportation with greater efficiency and zero carbon emission. The PVs on the other hand are source of clean and sustainable energy, which is generated everywhere, even in cities in order to support EV applications [1-4]. The PV module's output voltage is very low; so, the employment of an effective DC-DC converter for obtaining boosted voltage output is considered indispensable [5].

One of the most prevalently used converter for PV application is boost converter, which is used to perform the operation of voltage boosting with its simple design. However, it is not suitable for operations that require step-down voltage and is affected by excess amount of losses and voltage stress across the switches. The buck-boost converter, is able to perform both step-up and step-down voltage conversion, but on the downside, its output has inverted polarity in addition to discontinuous input current. The SEPIC converter, unlike a buck-boost converter, has a non-inverted output, continuous input current and isolates the output from the input via a series capacitor. It is also capable of providing both step-up and step-down voltage conversion ratios [6-9]. For the enhancement of the converter's dynamic properties in order to provide a stable and controlled output, the implementation of a proper controller is deemed necessary. The PI controller, due to its viable, robust and simple design along with greater stability margin, is one of the most frequently used controllers in wide range of operating situations [10]. On the downside, under varied operating conditions, the fixed PI control gain values have a substantial oscillations and peak overshoot in addition to delayed dynamic response. So, owing to the

 https://doi.org/10.37896/pd91.4/9149

ISSN: 0369-8963

uncertainties and nonlinearities innate to the PV system, the process of tuning their parameters is considered difficult [11]. This drawback of a PI controller is solved by the application of optimization techniques for effective tuning of PI parameters. The optimization techniques aids in determining the most efficient use of existing resources in obtaining a solution while eliminating any limits that may exist. Several metaheuristic optimization techniques such as Genetic Algorithm [12], Particle Swarm Optimization [13, 14], Grey Wolf Optimization [15], etc are proposed for tuning PI parameters. Genetic dynamics concepts are at the core of GA and the effectiveness of such a strategy is largely dependent on accurate population coding. Although the PSO algorithm is simple in design and has fewer configurable parameters, it still has issues such as delayed convergence and trapped in local optima. Hence, this research proposes an improved particle swarm optimization integrated grey wolf optimization (GWO-PSO). During iteration, the GWO can sort the particles to discover the ones with the best fitness value and direct other particles to them, thus bringing considerable improvement in the searching capability of PSO. The most efficient motor for EV application is BLDC motor because it has simple design, excellent speed-torque characteristics, and lower maintenance in addition to broad range of speed [16-18]. For the speed regulation of BLDC motor, a PI controller is adopted in this work.

A PV based EV charging system is proposed in this work, where the required power to run the BLDC motor of EV, is supplied from the PV through a SEPIC converter and 3φ VSI. The SEPIC converter is controlled using a GWO-PSO optimized PI controller. By the employment of a PI controller, the effective regulation of the BLDC motor's speed is ensured. The BLDC motor is power by the grid through a 1φVSI, during the absence of photo generated current.

PROPOSED METHODOLOGY

Currently the world is focusing on the development of a sustainable and decarbonised transportation and energy generation system due to uncertainity that persists around the fossil fuel availability along with the need to tackle climate change and global warming. A PV based EV charging system is proposed in order to overcome the aforementioned issues. The most prominently used drive motor in EVs are BLDC motors owing to their enhanced efficiency, simple design, reduced losses, outstanding speed regulation capability and less maintenance requirement. Both the PV in addition to the electric grid aid in powering of the EV's BLDC motor. The low voltage output from the PV system is boosted to the desired level by the application of a SEPIC converter. The working of the converter is further enhanced with the employment of Hybrid GWO-PSO optimized PI controller. The desired reference voltage level is compared to the SEPIC converter's actual output voltage, and the obtained error value is given to the Hybrid GWO-PSO optimized PI controller. The Hybrid GWO-PSO algorithm combines the benefits of both the involved metaheuristic algorithms and successfully assists in the process of tuning of PI parameters. The output from the controller is supplied to the PWM generator, which in turn generates the required gating pulses that controls the switching operation of the converter. The steady voltage output from the SEPIC converter is fed to the 3φ VSI, which consequently powers the BLDC motor of the EV. Figure 1 presents the proposed PV based EV charging system.

 https://doi.org/10.37896/pd91.4/9149

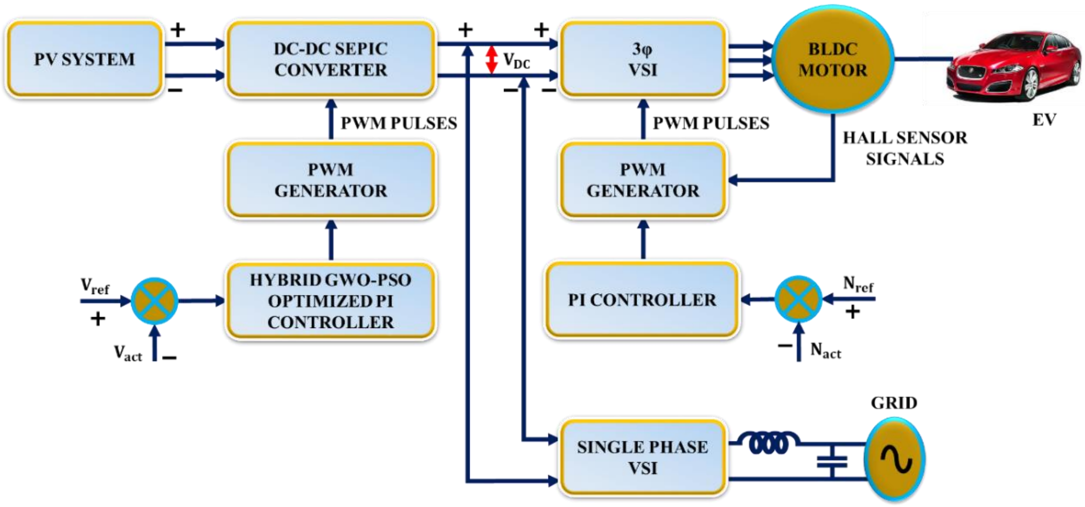

Figure 1 PV based EV with Hybrid optimized PI and SEPIC converter

The BLDC motor's speed is kept under control by a PI controller. The error signal is provided to the PI controller after the reference speed N_{ref} is compared to the actual motor speedN_{act}. The controller output enables the PWM generator to produce pulses for controlling the switching operation of the 3φ VSI. Hence through the effective control of voltage and frequency of the 3φ VSI, the speed control of BLDC motor is accomplished. Hall sensor is used to estimate the position of the rotor for determining the commutation, in order to control a BLDC motor. During daytime, power for BLDC motor comes from the PV system, however at night the power for the EV comes from the grid. The grid is connected to the system through a 1φ VSI.

PROPOSED SYSTEM MODELLING

A) PV SYSTEM MODELLING:

For obtaining the essential level of current or voltage levels, numerous PV cells are coupled in series and parallel combination in a PV module. Basically, the PV cell is a p-n junction semiconductor diode of large area. Figure 2 illustrates a simple PV cell equivalent circuit based on single diode model.

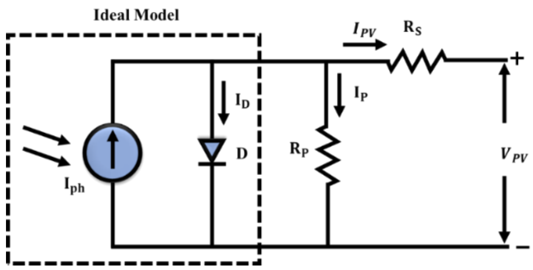

Figure 2 Single diode model of PV cell

The circuit of the PV cell in general comprises of light-generated current I_{ph}, series resistance R_s that offers internal resistance to the flow of current, a diode D and a parallel resistance R_p. On applying Kirchhoff's current law, the acquired equation is,

$$I_{pv} = I_{ph} - I_D - I_p \quad (1)$$

ISSN: 0369-8963

Where, the terms I_D and I_P refers to the current flowing through the diode and shunt resistor respectively.

$$I_P = \frac{V_{pv}+R_S I_{pv}}{R_p} \tag{2}$$

$$I_D = I_{sd}\left(exp\left(\frac{qV_{pv}+R_S I_{pv}}{nKT}\right) - 1\right) \tag{3}$$

Where, the reverse saturation current is represented as I_{sd}, the terms K and q refers to the Boltzmann constant and electron charge respectively. The terms T and n refers to temperature and ideal factor respectively. By replacing the value of I_D in Eq (1).

$$I_{pv} = I_{ph} - I_{sd}\left(exp\left(\frac{qV_{pv}+R_S I_{pv}}{nKT}\right) - 1\right) - \frac{V_{pv}+R_S I_{pv}}{R_p} \tag{4}$$

The magnitude of the light generated current chiefly relies on temperature and radiation, which is given as,

$$I_{ph} = [I_{sc} + K_i(T - T_{ref})]\frac{G}{G_{ref}} \tag{5}$$

Where, I_{sc} is the short-circuit current, T_{ref} and K_i are the reference temperature and temperature coefficient respectively. The terms G and G_{ref} refers to the solar radiation and reference insolation respectively. The voltage output from the PV module is typically low and unregulated in nature, therefore a SEPIC converter is employed, in order to obtain a regulated and desired voltage output.

B) SEPIC CONVERTER:

The SEPIC converter, which is from the family of buck-boost converter is capable of generating a voltage output, which is lesser or higher than the given voltage input without the reversal of polarity. It is mainly composed of two capacitors, two inductors along with a diode and power switch. Figure 3 illustrates the SEPIC converter's equivalent circuit in addition to its two operational stages.

Stage 1: The switch is in ON condition and the diode is reverse biased, since the polarity of the coupling capacitor C_1 is negative. The capacitor C_1 discharges and the inductors L_1 and L_2 begins charging in this stage.

Stage 2: In this stage the diode is forward biased and begins conducting. The switch is turned OFF in this stage and both the inductors L_1 and L_2 discharges and its energy is transferred to the capacitor C_1 and load respectively.

 https://doi.org/10.37896/pd91.4/9149

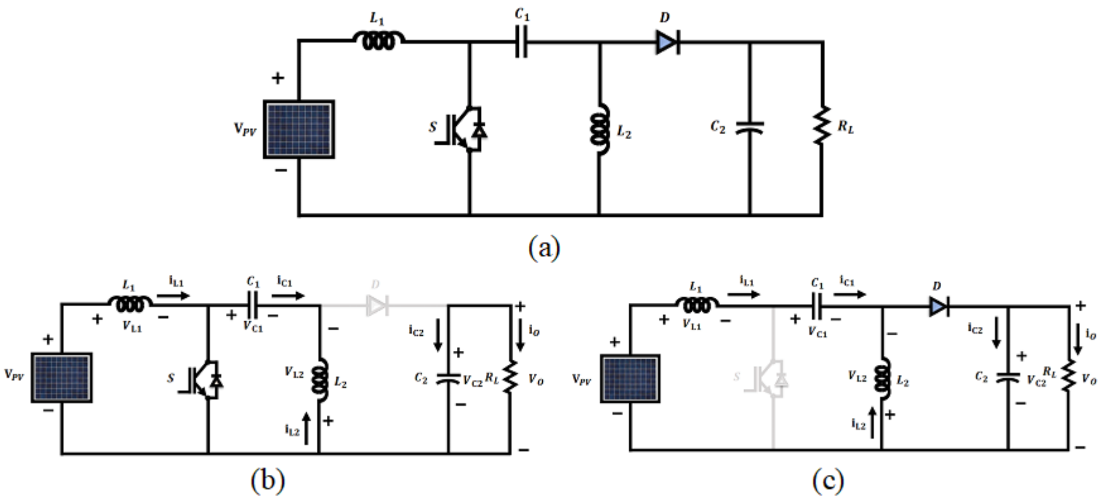

Figure 3 Equivalent circuit (a) SEPIC converter (b) Stage 1 and (c) Stage 2

The value of SEPIC converter's voltage gain is given as,

$$\frac{V_o}{V_{pv}} = \frac{D}{1-D} \tag{6}$$

Where the duty cycle D is given as,

$$D = \frac{V_o}{V_o+V_{PV}} \tag{7}$$

The values of inductor L_1 and L_2 is as follows,

$$L_1 = \frac{V_{pv}\times D}{\Delta i_{L_1}\times f_s} \tag{8}$$

$$L_2 = \frac{V_{pv}\times D}{\Delta i_{L_2}\times f_s} \tag{9}$$

The magnitude of the output voltage ripple is given as,

$$\Delta V_o = \Delta V_{C_2} = \frac{V_o D}{R C_2 f_s} \tag{10}$$

The equations that derive the value of capacitance $C_1$is given as,

$$C_1 = \frac{V_o\times D}{R\times\Delta V_{C_1}\times f_s} \tag{11}$$

The variation of voltage in capacitor C_1 is given as,

$$\Delta V_{C_1} = \frac{V_o D}{R C_1 f_s} \tag{12}$$

$$C_2 = \frac{V_o\times D}{R\times\Delta V_o\times f_s} \tag{13}$$

For obtaining a stable and steady DC output, a Hybrid GWO-PSO optimized PI controller is adopted in this work.

C) Hybrid GWO-PSO Optimized PI controller

The optimization algorithms are generally devised for determining the most effective controller parameters, which aids in providing optimal response for maintaining a stable operation. Here a hybrid GWO-PSO algorithm is adopted for parameter tuning of PI controller.

 https://doi.org/10.37896/pd91.4/9149

The PSO algorithm is a smart population-based optimization method derived from the research on life habits of flocks of animals. It comprises of a swarm of particles, each of which is assigned a velocity vector v_t and a position vector x_t. Figure 4 presents the flowchart and particle displacement in a PSO. The scale of the search space is equal to the size of these vectors. At an iteration t, the velocity v_t denotes the directional distance travelled by the particle in the $(t-1)^{th}$ iteration. A particle's directional velocity is calculated using the particle's personal best ($pbest$) (p_l) and swarm's global best ($gbest$) (p_g).

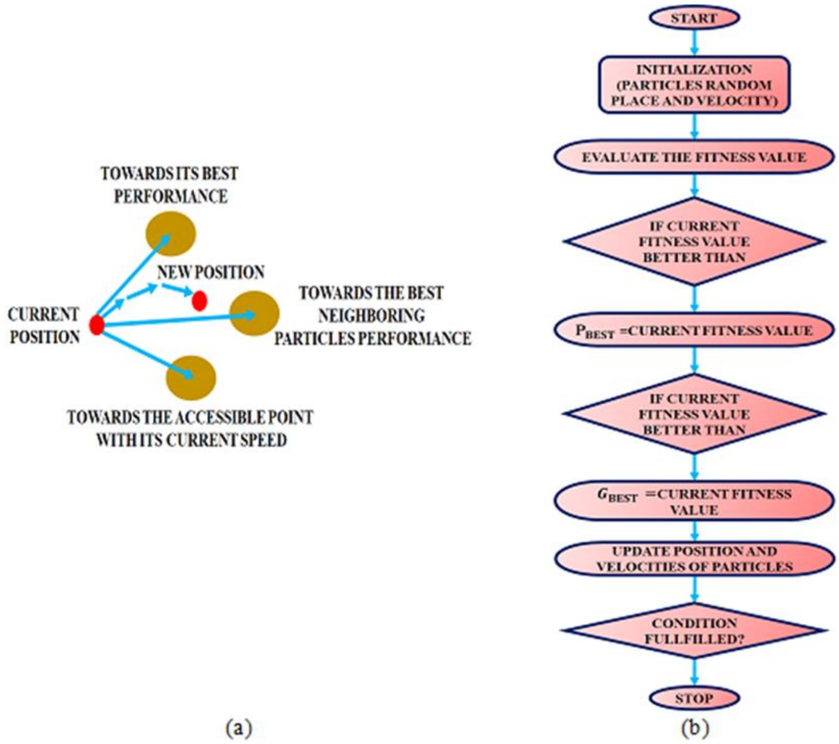

Figure 4 PSO (a) Displacement of particle and (b) Flowchart

At any iteration, the position and velocity update of ith particle is given as,

$$v_{i,t+1} = wv_{i,t} + c_1r_1.*\left(p_{l,i} - x_{i,t}\right) + c_2r_2.*\left(p_g - x_{i,t}\right) \tag{14}$$

Where, the random vectors within the range [0, 1] is $r_1 and\ r_2$ and the pre-specified constants are represented as $w, c_1 and\ c_2$. The particle's next location is determined based on its current velocity and previous location.

$$x_{i,t+1} = x_{i,t} + v_{i,t+1} \tag{15}$$

GWO is another optimization algorithm, which is derived based upon the social intelligence and hierarchical behaviour of the wolves to determine the global optimal solution. The overall hunting operation is accomplished together by four types of wolves, each having its own distinct function. The Alphas are the ones in charge of the entire hunting process, makes the decision and others comply. The beta comes next in the hierarchy, trailed by delta at next and then by omega. Three major steps that together contribute to the wolf pack's hunting process : chasing, surrounding, and attacking the prey. Figure 5 illustrates the hierarchy level of grey wolves in addition to the flowchart of GWO.

 https://doi.org/10.37896/pd91.4/9149

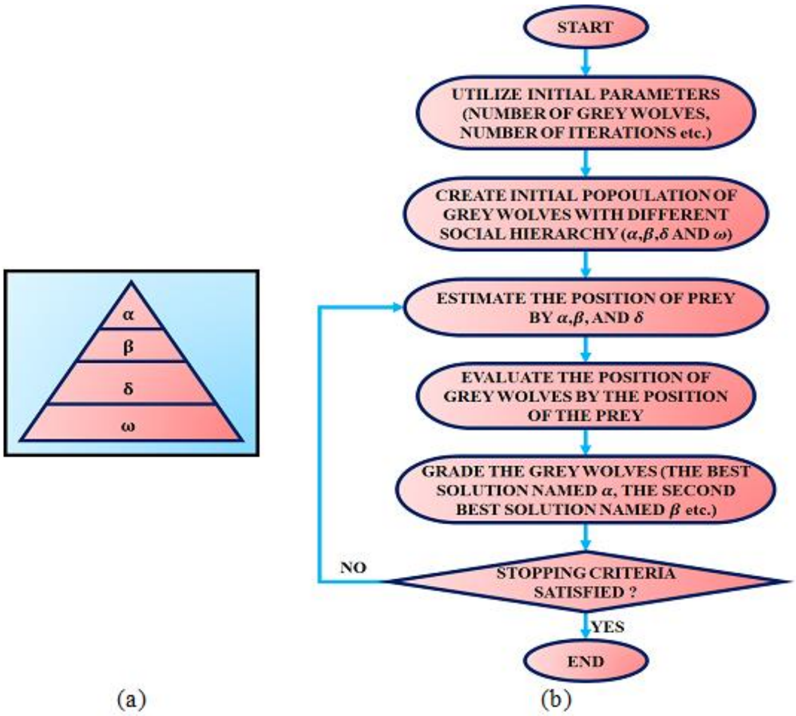

Figure 5 GWO (a) Hierarchy level and (b) GWO flowchart

The process starts with a set number of grey wolves, whose locations are randomly created. The position change of the wolves while attacking is given as,

$$\vec{D} = \left|\vec{C}.\overrightarrow{X_p}(t) - \overrightarrow{X(t)}\right| \quad (16)$$

$$\vec{X}(t+1) = \overrightarrow{X_p}(t) - \vec{A}.\vec{D} \quad (17)$$

Here, vector position of grey wolf and its prey is specified as $\overrightarrow{X(t)}$ and $\overrightarrow{X_p}(t)$ respectively. The subsequent equations give the value of vectors $\vec{A}$ and $\vec{C}$,

$$\begin{cases} \vec{A} = 2.\vec{a}.\overrightarrow{r_1} - \vec{a} \\ \vec{C} = 2.\overrightarrow{r_2} \end{cases} with: a = 2.\left(1 - \frac{t}{T_{max}}\right) \quad (18)$$

Where, the total iteration and current iteration is specified as T_{max} and t respectively. The random vectors within the interval [0, 1] is specified as r_1 and r_2. The updated position of the prey $\overrightarrow{X_p}(t+1)$is computed by determining the average of positions of $\alpha, \beta\ and\ \Delta$ wolves, which is given as,

$$\overrightarrow{X_p}(t+1) = \frac{\overrightarrow{X_1}(t)+\overrightarrow{X_2}(t)+\overrightarrow{X_3}(t)}{3} \quad (19)$$

Where, $\begin{cases} \overrightarrow{X_1}(t) = \overrightarrow{X_\alpha}(t) - \overrightarrow{A_1}.\overrightarrow{D_\alpha} \\ \overrightarrow{X_2}(t) = \overrightarrow{X_\beta}(t) - \overrightarrow{A_2}.\overrightarrow{D_\beta} \\ \overrightarrow{X_3}(t) = \overrightarrow{X_\delta}(t) - \overrightarrow{A_3}.\overrightarrow{D_\delta} \end{cases}$ and $\begin{cases} \overrightarrow{D_\alpha} = \left|\vec{C}_1\vec{X}_\alpha(t) - \vec{X}(t)\right| \\ \overrightarrow{D_\beta} = \left|\vec{C}_2\vec{X}_\beta(t) - \vec{X}(t)\right| \\ \overrightarrow{D_\delta} = \left|\vec{C}_3\vec{X}_\delta(t) - \vec{X}(t)\right| \end{cases}$

The distance from the present location $\vec{D}$ needs to be reduced as short as possible, therefore Eq (17), which represents the next position is as close as possible to the prey. Thus,

 https://doi.org/10.37896/pd91.4/9149

the accurate solution to the problem $X_p(t)$ is attained. Figure 6 gives the flowchart of hybrid GWO-PSO.

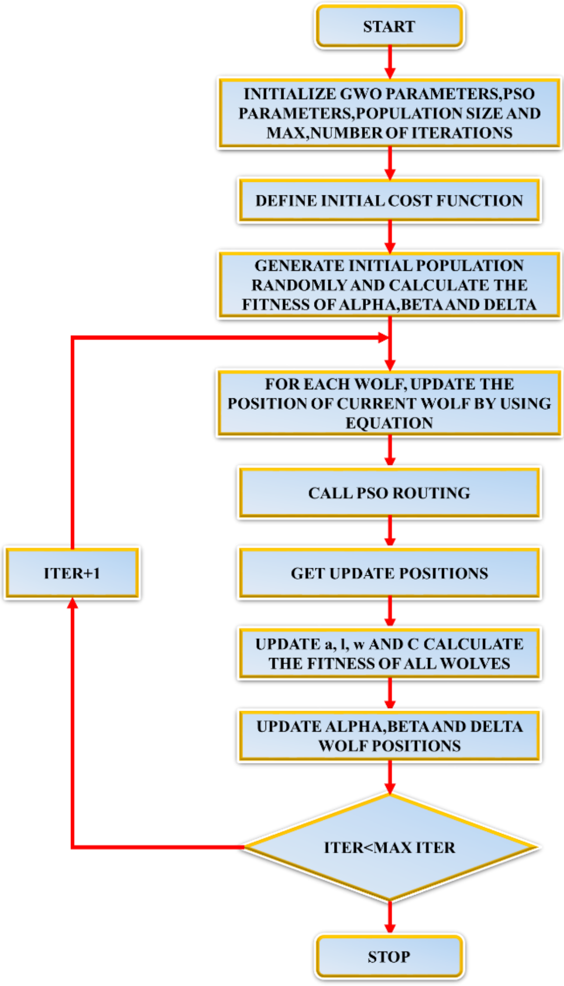

Figure 6 Hybrid GWO-PSO flowchart

By the adoption of a hybrid algorithm, the benefits of both PSO and GWO can be combined and the global best solution is achieved with enhanced convergence rate, quantity and time. With GWO, the exploration strategy is improved because the wolves explore the search space effectively. PSO, on the other hand, aids in improving exploitation so that convergence to the solution and the global optimum can be obtained in a timely manner. Exploration and exploitation are carried out in a balanced manner. Thus the performance of both the techniques are complemented and strengthened by subduing the issues associated with convergence rate and local stagnation. By using inertial weight constants, the variations are made in the subsequent equations. In order to better the exploration process, initially the improvement of search agent position is carried out. The inertia constant was introduced to govern the wolves' attacking and surveying activities, which is given as,

$$\vec{D}_\alpha = \left|\vec{C_1}.\vec{X_\alpha}(t) - w * \vec{X}(t)\right| \tag{20}$$

$$\vec{D}_\beta = \left|\vec{C_1}.\vec{X_\beta}(t) - w * \vec{X}(t)\right| \tag{21}$$

$$\vec{D}_\delta = \left|\vec{C_1}.\vec{X_\delta}(t) - w * \vec{X}(t)\right| \tag{22}$$

https://doi.org/10.37896/pd91.4/9149

ISSN: 0369-8963

The velocity and revised position of the search agents for improving the PSO's exploitation capacities is given as,

$$v_{i,t+1} = w * \{v_{i,t} + c_1 r_1.* \left(p_1 - x_{i,t}\right) + c_2 r_2.* \left(p_2 - x_{i,t}\right) + c_3 r_3.* \left(p_3 - x_{i,t}\right)\} \tag{23}$$

$$x_{i,t+1} = x_{i,t} + v_{i,t+1} \tag{24}$$

The proposed Hybrid GWO-PSO pseudo code is expressed as,

$Initialization$

$Initialize\ l, a, w\ and\ c$

$//w\ =\ 0.5\ +\ rand\ ()/2$

$Evaluate\ the\ fitness\ of\ agents\ by\ using\ v_{i,t+1}$
$= wv_{i,t} + c_1 r_1.* \left(p_{l,i} - x_{i,t}\right) + c_2 r_2.* \left(p_g - x_{i,t}\right)$

$while\ (t\ <\ max\ no\ of\ iter)$

$for\ each\ search\ agent$

$Update\ the\ velocity\ and\ position\ by\ using\ x_{i,t+1} = x_{i,t} + v_{i,t+1}$

$end\ for$

$Update\ l, a, w\ and\ c$

$Evaluate\ the\ fitness\ of\ all\ search\ agents$

$Update\ position\ first\ three\ agents$

$t = t + 1$

$end\ while$

$return\ //\ first\ best\ search\ agent\ position$

The output from the GWO-PSO algorithm is used for effective tuning of both K_P and K_I values of the PI controller, which controls the switching operation of the SEPIC converter.

D) Modelling of BLDC motor

The steady output from the SEPIC converter is fed to the 3φ VSI, whereas, the output from the 3φ VSI is used to power the BLDC motor. The BLDC motor has a configuration equivalent to that of a permanent magnet synchronous motor, which consists primarily of a rotor with permanent magnet pole and stator with armature winding. The hall sensor provides the accurate commutation information to PWM generator by detecting the location of the magnetic pole of the rotor. The equivalent circuit and mechanical model of a BLDC motor is shown in Figure 7. The rotor position along with the back-emf current and voltage representation is presented in Figure 8.

 https://doi.org/10.37896/pd91.4/9149

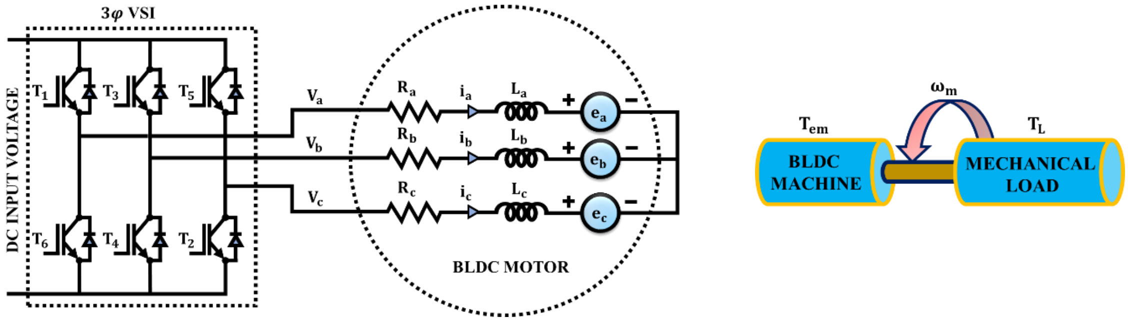

(a) (b)

Figure 7 BLDC motor (a) equivalent circuit and (b) mechanical model

The voltage equations attained by the application of Kirchhoff's law to the 3φ stator windings gives,

$$V_a = R_a i_a + L_a \frac{di_a}{dt} + M_{ab}\frac{di_b}{dt} + M_{ac}\frac{di_c}{dt} + e_a \tag{25}$$

$$V_b = R_b i_b + L_b \frac{di_b}{dt} + M_{ba}\frac{di_a}{dt} + M_{bc}\frac{di_c}{dt} + e_b \tag{26}$$

$$V_c = R_c i_c + L_c \frac{di_c}{dt} + M_{ca}\frac{di_a}{dt} + M_{cb}\frac{di_b}{dt} + e_c \tag{27}$$

The mathematical model of the BLDC motor is,

$$\begin{bmatrix} L_a & M_{ab} & M_{ac} \\ M_{ba} & L_b & M_{bc} \\ M_{ca} & M_{cb} & L_c \end{bmatrix} \frac{d}{dt}\begin{bmatrix} i_a \\ i_b \\ i_c \end{bmatrix} = \begin{bmatrix} V_a \\ V_b \\ V_c \end{bmatrix} - \begin{bmatrix} R_a & 0 & 0 \\ 0 & R_b & 0 \\ 0 & 0 & R_c \end{bmatrix}\begin{bmatrix} i_a \\ i_b \\ i_c \end{bmatrix} - \begin{bmatrix} e_a \\ e_b \\ e_c \end{bmatrix} \tag{28}$$

Where, e_a, e_b, e_c represents the back emf; V_a, V_b, V_c represents the voltages of phases a, b and c; $R= R_a=R_b=R_c$ represents the end resistance; $L=L_a=L_b=L_c$ represents self-inductance and the terms $M=M_{ab}=M_{ac}=M_{ba}=M_{bc}=M_{ca}=M_{cb}$ represents the mutual inductance. After the rearrangement of the above equation,

$$\begin{bmatrix} L & M & M \\ -M & L & M \\ M & M & L \end{bmatrix} \frac{d}{dt}\begin{bmatrix} i_a \\ i_b \\ i_c \end{bmatrix} = \begin{bmatrix} V_a \\ V_b \\ V_c \end{bmatrix} - \begin{bmatrix} R & 0 & 0 \\ 0 & R & 0 \\ 0 & 0 & R \end{bmatrix}\begin{bmatrix} i_a \\ i_b \\ i_c \end{bmatrix} - \begin{bmatrix} e_a \\ e_b \\ e_c \end{bmatrix} \tag{29}$$

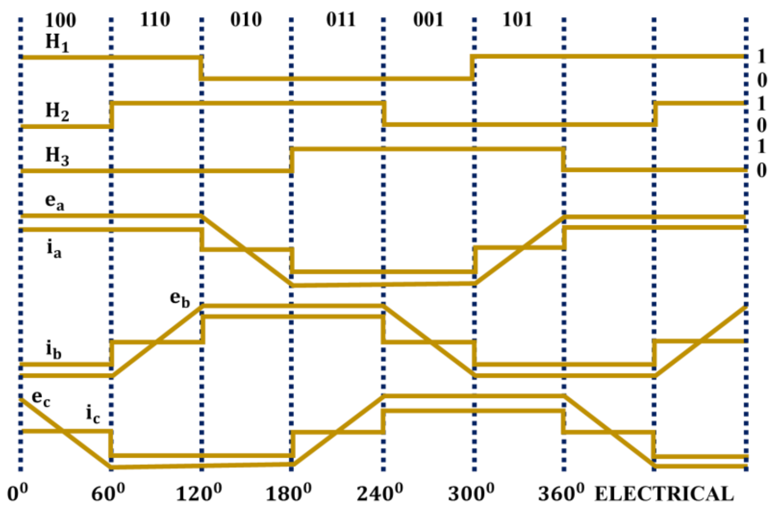

 https://doi.org/10.37896/pd91.4/9149

Figure 8 Back-emf current and voltage in addition to rotor position for each phase

The torque equation is given as,

$$T_{em} = J\frac{d\omega_r}{dt} + B\omega_r + T_L \tag{30}$$

The 3φ BLDC motor's electromagnetic torque relies on speed, current and back-emf, so the value of instantaneous electromagnetic torque is given as,

$$T_{em} = \frac{1}{\omega_m}(e_a i_a + e_b i_b + e_c i_c) \tag{31}$$

A PI controller is used to regulate the motor speed of the BLDC motor. For motor speed control, a constant volts/hertz ratio needs to be maintained. The voltage input of the 3φ VSI is maintained stable using the hybrid GWO-PSO optimized PI controller-based SEPIC converter. Figure 9 presents the structure of a PI controller.

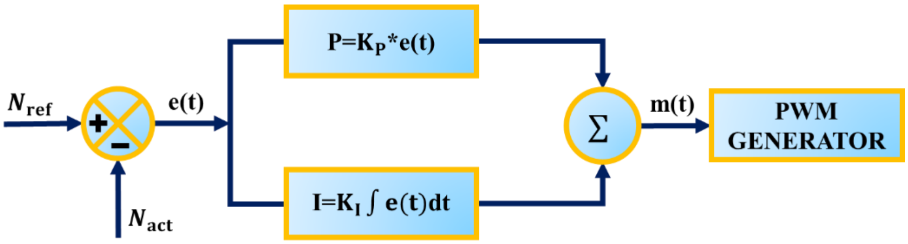

Figure 9 Structure of PI controller

The reference speed N_{ref} is compared to the actual speed N_{act} of the BLDC motor and the obtained error signal is fed to the PI controller. The acquired output from the controller is used to control the 3φ VSI's switching operation through the pulses generated by a PWM generator. Thus, the PI controller is used for the effective control of frequency of the 3φ VSI's output. The BLDC motor is powered with a regulated and controlled voltage and frequency input and the speed control of BLDC motor is ensured.

E) SINGLE PHASE VSI

The excess power from the PV furnishes the grid and when the PV generated power is not available, the supply for EV charging is derived from the grid. A ceaseless supply of power is always provided to the EV charging system. Figure 10 presents the structure of 1φ VSI connected to the utility grid.

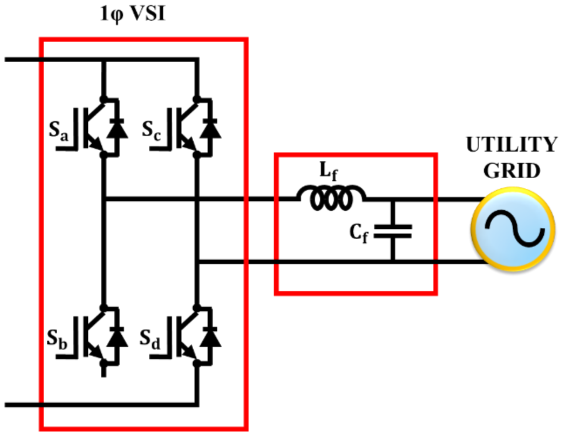

Figure 10 Grid connected 1φ VSI

 https://doi.org/10.37896/pd91.4/9149

Through a 1φ VSI, the utility grid is interfaced to EV charging system. The harmonic contents present in the inverter output is reduced using a LC filter and is then fed to AC grid. The general purpose of an inverter is to provide the utility grid with AC supply by transforming its input DC supply. By considering the inverter's voltage output and the phase of grid voltage, the process of grid synchronization is achieved.

RESULTS AND DISCUSSIONS

An effective hybrid optimization algorithm for PV based EV charging system using SEPIC converter is discussed in this work. In this section, the adopted control technique is validated using MATLAB, and the results are presented in detail. Table 1 lists the parameters of the solar panel and SEPIC converter used in the simulation.

Parameters	Values
PV Panel	
Peak power	100W, 15 Panels
Short circuit current I_{SC}	5.86 A
Open circuit voltage V_{OC}	22.68 V
Number of series connected PV cells N_s	36
SEPIC converter	
Switching Frequency	10 KHz
L_1, L_2	0.288mH
C_1, C_2	150µF
Diode	MCD95

Table 1 PV panel and SEPIC converter specifications

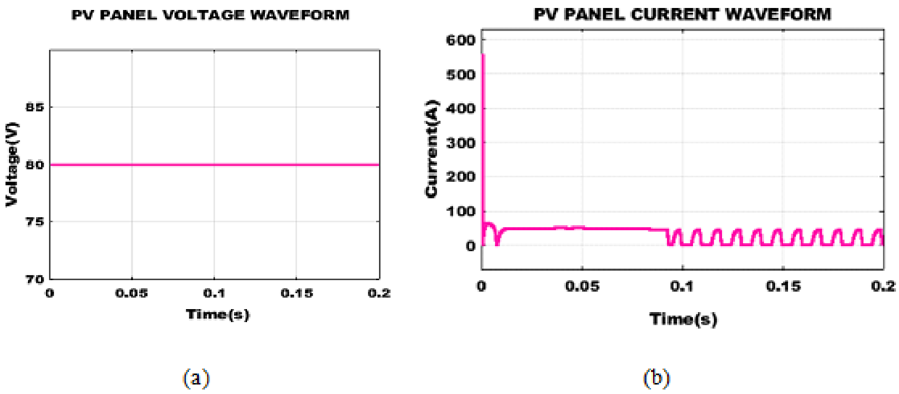

Figure 11 PV panel (a) Voltage waveform and (b) Current waveform

The simulation waveform, which represents the PV panel output voltage and current is presented in Figure 11. From the PV panel, a voltage of 80V is obtained. The effects of variations in operating conditions of the PV system is reflected in the current waveform, since incessant fluctuation in the amplitude of PV generated current is witnessed from 0.09sec to 0.2sec. The PV current of 50A is obtained from the PV panel.

 https://doi.org/10.37896/pd91.4/9149

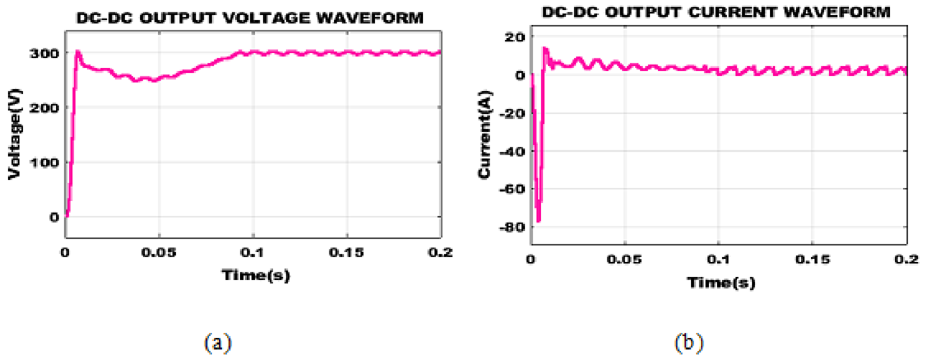

Figure 12 Output of SEPIC based on PI (a) Voltage waveform and (b) Current waveform

The waveforms that represent the voltage and current output of the SEPIC converter controlled by a PI controller is presented in Figure 12. The voltage output of the converter, is initially affected by peak overshoot issues and a voltage of 300V is achieved at 0.1sec. However the obtained voltage is not stable and is highly affected by oscillations.

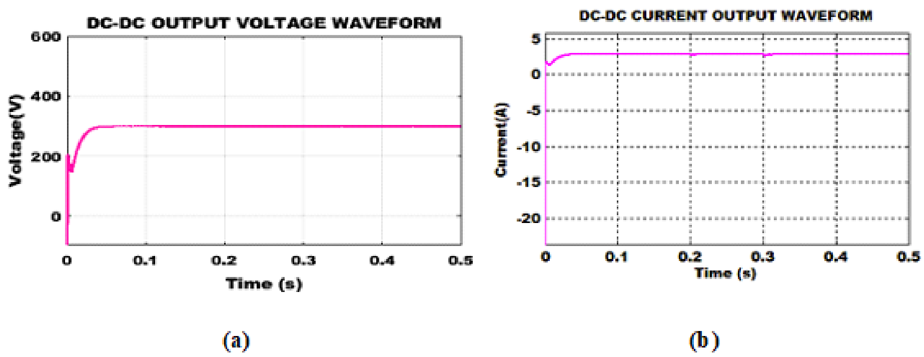

Figure 13 Output of SEPIC converter using Hybrid GWO-PSO optimized PI controller (a) Voltage waveform and (b) Current waveform

The converter output using Hybrid GWO-PSO optimized PI controller is illustrated in Figure 13. Unlike the conventional PI controller, the proposed Hybrid GWO-PSO optimized PI controller is successful in eliminating the problem of peak overshoot. A constant and steady voltage of 300V is obtained within a quick setting time of 0.03 sec. The output current of the converter becomes stable at 0.03sec and a steady current of 3A is acquired from the converter. Thus, the suggested control method is capable of overcoming the PV system's non-linear nature by maintaining a constant power supply.

https://doi.org/10.37896/pd91.4/9149

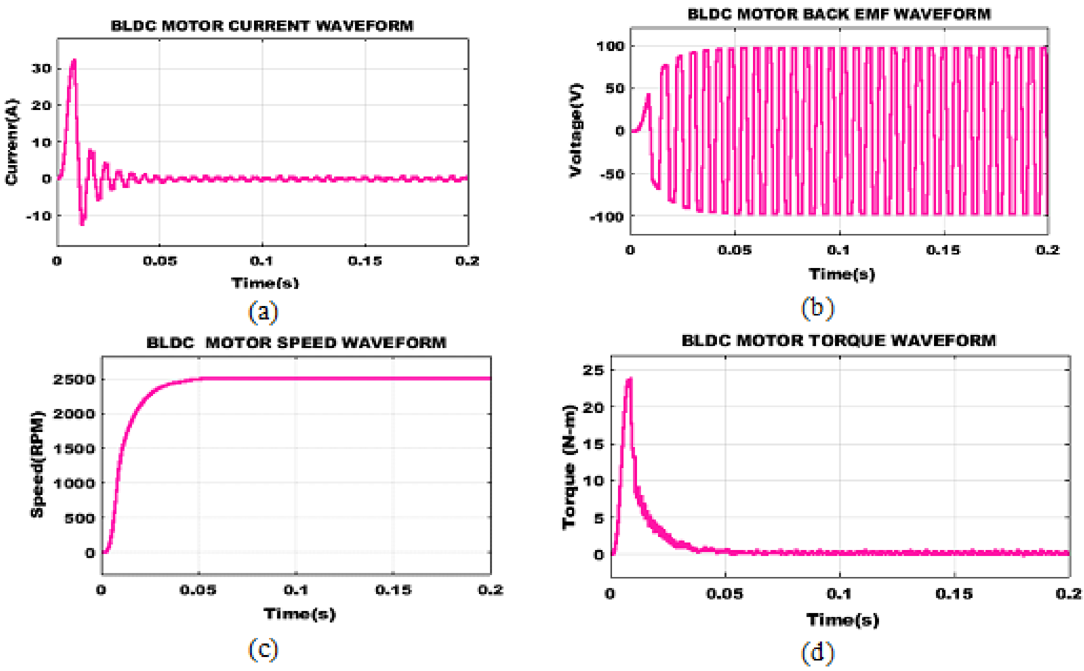

Figure 14 BLDC motor (a) Current waveform (b) waveform of Back EMF (c) waveform for Speed and (d) waveform for Torque

The simulation outputs of the BLDC motor is given in Figure 14. The BLDC motor draws excess amount of current when it starts and then from 0.05sec, it draws a minimum current of 2A. The BLDC motor runs at a stable speed of 2500rpm from 0.05sec, hence the back-emf of the motor also stabilizes at a magnitude of 100V from 0.05sec. The initial torque will be higher as the motor consumes more current during the initial stages. From 0.05sec, the motor torque becomes 1Nm.

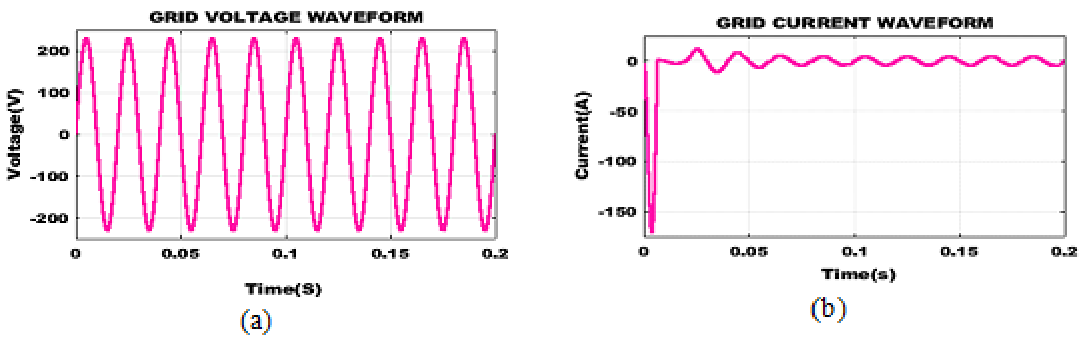

Figure 15 Power grid (a) Voltage waveform and (b) Current waveform

From the waveforms that depict the grid voltage and current, it is noted that a constant voltage of 230V and 5A is supplied to the grid. The grid current takes 0.05sec to become stable at magnitude 5A.

 https://doi.org/10.37896/pd91.4/9149

ISSN: 0369-8963

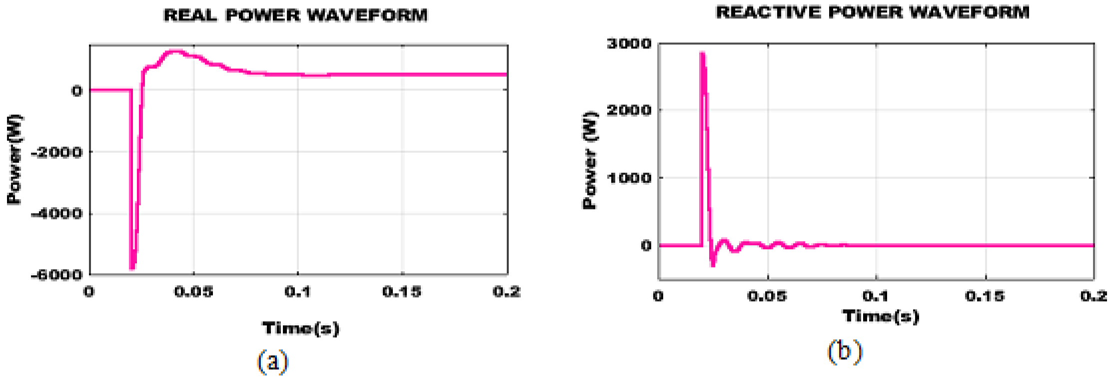

Figure 16 1φ grid **(a)** Real Power and **(b)** Reactive Power

The waveforms illustrating the real and reactive power of the 1φ grid is presented in Figure 16. The magnitude of real power becomes a stable value of 500W at 0.08sec, whereas the magnitude of reactive power after reaching a peak value of 2800W, decreases to a negligible value from 0.08sec. The SEPIC converter with an efficiency of 95% and voltage gain of 1:8, gives better results on comparison with other conventional converters as presented in Figure 17.

Table 2 DC-DC converter efficiency and Voltage gain comparison

Converter	Efficiency	Voltage gain
Buck-Boost	86%	1:1.5
Boost	83.54%	1:3
Cuk	89.40%	1:4
SEPIC	95%	1:8

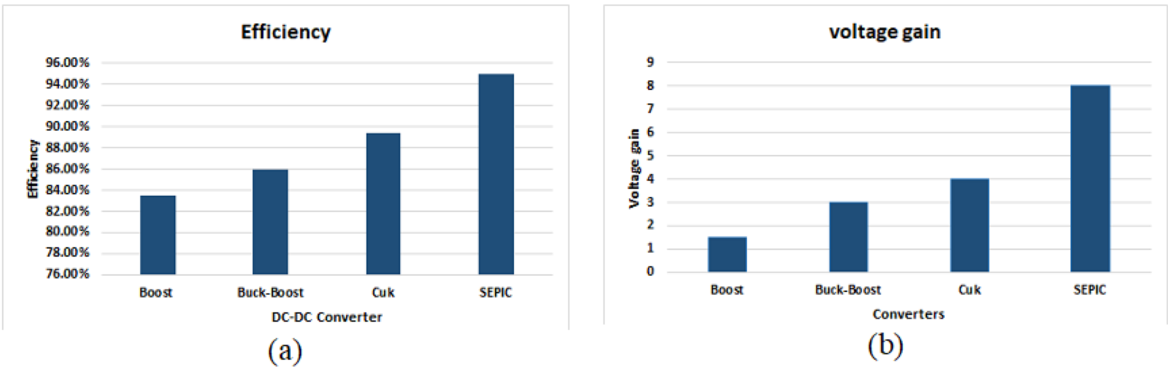

Figure 17 DC-DC converters (a) Efficiency comparison and (b) Voltage gain comparison

https://doi.org/10.37896/pd91.4/9149

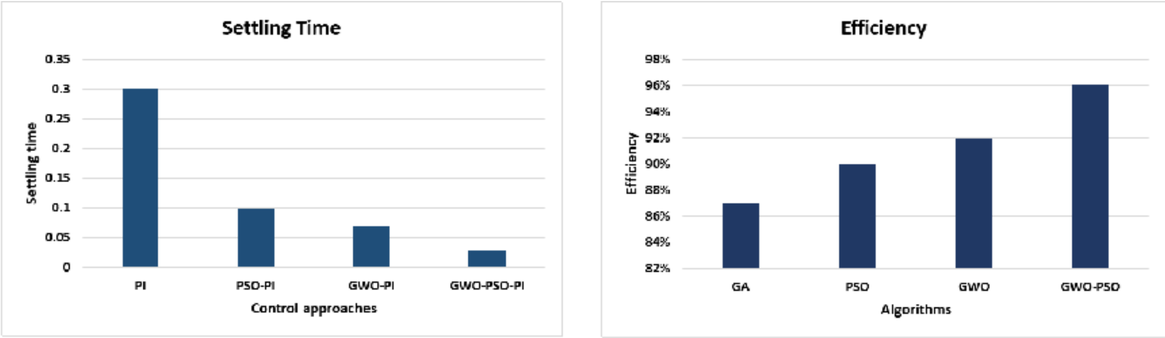

(a) (b)

Figure 18 (a) Settling time comparison and (b) Efficiency comparison

The proposed Hybrid GWO-PSO optimized PI controller is effective in operating with an improved efficiency of 96% and minimized settling time of 0.3s as shown in Figure 18.

CONCLUSION

This paper discusses a hybrid optimization approach for a PV-based EV charging system employing a SEPIC converter. PV-based EV have attracted considerable attention since they promote sustainable transportation while addressing climate change with reduced carbon footprint. A SEPIC converter regulates and boosts the PV system output with an enhanced efficiency of 95%. By producing gate pulses from PWM, the GWO-PSO optimized PI controller with an efficiency of 96%, contributes to the enhancement of the switching state of the SEPIC converter in addition to quicker settling times. The adoption of grid tied PV ensures continuous supply of power for EV even during night time. As a result, by maintaining a steady power supply, the control technique adopted is able to transcend the non-linear behaviour of the PV system.

REFERENCES

1. G. R. Chandra Mouli, M. Kefayati, R. Baldick and P. Bauer, "Integrated PV Charging of EV Fleet Based on Energy Prices, V2G, and Offer of Reserves," in *IEEE Transactions on Smart Grid*, vol. 10, no. 2, pp. 1313-1325, March 2019.

2. G. R. Chandra Mouli, M. Kefayati, R. Baldick and P. Bauer, "Integrated PV Charging of EV Fleet Based on Energy Prices, V2G, and Offer of Reserves," in *IEEE Transactions on Smart Grid*, vol. 10, no. 2, pp. 1313-1325, March 2019.

3. N. Liu, Q. Chen, X. Lu, J. Liu and J. Zhang, "A Charging Strategy for PV-Based Battery Switch Stations Considering Service Availability and Self-Consumption of PV Energy," in *IEEE Transactions on Industrial Electronics*, vol. 62, no. 8, pp. 4878-4889, Aug. 2015.

4. K. Chaudhari, A. Ukil, K. N. Kumar, U. Manandhar and S. K. Kollimalla, "Hybrid Optimization for Economic Deployment of ESS in PV-Integrated EV Charging Stations," in *IEEE Transactions on Industrial Informatics*, vol. 14, no. 1, pp. 106-116, Jan. 2018.

5. M. Forouzesh, Y. Shen, K. Yari, Y. P. Siwakoti and F. Blaabjerg, "High-Efficiency High Step-Up DC–DC Converter With Dual Coupled Inductors for Grid-Connected Photovoltaic Systems," in *IEEE Transactions on Power Electronics*, vol. 33, no. 7, pp. 5967-5982, July 2018

6. K. Nathan, S. Ghosh, Y. Siwakoti and T. Long, "A New DC–DC Converter for Photovoltaic Systems: Coupled-Inductors Combined Cuk-SEPIC Converter," in *IEEE Transactions on Energy Conversion*, vol. 34, no. 1, pp. 191-201, March 2019

 https://doi.org/10.37896/pd91.4/9149

7. A. El Khateb, N. A. Rahim, J. Selvaraj and M. N. Uddin, "Fuzzy-Logic-Controller-Based SEPIC Converter for Maximum Power Point Tracking," in *IEEE Transactions on Industry Applications*, vol. 50, no. 4, pp. 2349-2358, July-Aug. 2014.

8. G. Wu, X. Ruan and Z. Ye, "Nonisolated High Step-Up DC–DC Converters Adopting Switched-Capacitor Cell," in *IEEE Transactions on Industrial Electronics*, vol. 62, no. 1, pp. 383-393, Jan. 2015

9. B. Chandrasekar et al., "Non-Isolated High-Gain Triple Port DC–DC Buck-Boost Converter With Positive Output Voltage for Photovoltaic Applications," in IEEE Access, vol. 8, pp. 113649-113666, 2020.

10. M. S. Ali, L. Wang, H. Alquhayz, O. U. Rehman and G. Chen, "Performance Improvement of Three-Phase Boost Power Factor Correction Rectifier Through Combined Parameters Optimization of Proportional-Integral and Repetitive Controller," in *IEEE Access*, vol. 9, pp. 58893-58909, 2021.

11. K. Y. Ahmed, N. Z. Bin Yahaya, V. S. Asirvadam, N. Saad, R. Kannan and O. Ibrahim, "Development of Power Electronic Distribution Transformer Based on Adaptive PI Controller," in *IEEE Access*, vol. 6, pp. 44970-44980, 2018.

12. Hassan, Lokman & Moghavvemi, Mahmoud & Almurib, Haider & Muttaqi, Kashem & Ganapathy, V. Optimization of power system stabilizers using participation factor and genetic algorithm. International Journal of Electrical Power & Energy Systems, 2014.

13. D. Upadhyay, M. Ali, M. Tariq, S. A. Khan, B. Alamri and A. Alahmadi, "Thirteen-Level UXE-Type Inverter With 12-Band Hysteresis Current Control Employing PSO Based PI Controller," in *IEEE Access*, vol. 10, pp. 29890-29902, 2022.

14. V. Veerasamy *et al*., "A Hankel Matrix Based Reduced Order Model for Stability Analysis of Hybrid Power System Using PSO-GSA Optimized Cascade PI-PD Controller for Automatic Load Frequency Control," in *IEEE Access*, vol. 8, pp. 71422-71446, 2020.

15. K. C. and U. M. G., "Design of Gray Wolf Optimizer Algorithm-Based Fractional Order PI Controller for Power Factor Correction in SMPS Applications," in *IEEE Transactions on Power Electronics*, vol. 35, no. 2, pp. 2100-2118, Feb. 2020.

16. X. Nian, F. Peng and H. Zhang, "Regenerative Braking System of Electric Vehicle Driven by Brushless DC Motor," in *IEEE Transactions on Industrial Electronics*, vol. 61, no. 10, pp. 5798-5808, Oct. 2014.

17. A. Dadashnialehi, A. Bab-Hadiashar, Z. Cao and R. Hoseinnezhad, "Reliable EMF-Sensor-Fusion-Based Antilock Braking System for BLDC Motor In-Wheel Electric Vehicles," in *IEEE Sensors Letters*, vol. 1, no. 3, pp. 1-4, June 2017.

18. F. Naseri, E. Farjah and T. Ghanbari, "An Efficient Regenerative Braking System Based on Battery/Supercapacitor for Electric, Hybrid, and Plug-In Hybrid Electric Vehicles With BLDC Motor," in *IEEE Transactions on Vehicular Technology*, vol. 66, no. 5, pp. 3724-3738, May 2017.

AUTHOR DETAILS

[1]**KAVIN K S** was born in Kanyakumari, India. He received his Bachelor of Engineering degree in Electrical and Electronics Engineering from CSI Institute of Technology, Nagercoil, India, in 2009 under Anna University; and his Master of Engineering degree in Power Electronics and Drives from Anna University (Shanmuganathan Engineering College, Pudukkottai), India, in 2014. He is presently working towards his full time Ph.D. degree at Anna University, Chennai, India. His current research interests include BLDC Motors, shunt active filters, and DC-DC Converters.

[2]**Dr.SUBHA KARUVELAM P** was born in Tirunelveli, India. She received her Bachelor of Engineering degree in Electrical and Electronics Engineering from PSG College of technology, Coimbatore and Master of Engineering degree in Power Electronics and Drives from Government College of Engineering, Tirunelveli, India, in 1996 and 2005, respectively. She received her Ph.D. degree in Electrical Engineering from Anna University, Chennai, India, in 2015. In 2001 she joined Government College of Engineering, Tirunelveli, India, as a Professor in the Department of Electrical and Electronics Engineering, where she was an Assistant Professor from 2001 to 2018, and Associate Professor from 2019 to till date. Her current research interests include intelligent control techniques, power quality monitoring, power electronic converters and AC drives. She has published more than 20 technical papers in national and international journals.

[3]**Dr.M.GNANA SUNDARI** received her B.E degree in Electrical and Electronics Engineering in the year 1997 and M.E degree in Power Electronics and Drives in the year 2005 from Government College of Engineering, Tirunelveli, India affiliated to Anna University Chennai. She received her PhD degree from Anna University, Chennai, in the year 2016. She is currently a Professor in Government College of Engineering, Tirunelveli. Her research interests include intelligent control techniques, power quality monitoring and power electronic converters. She has published around 10 research articles in national and international journals.

 https://doi.org/10.37896/pd91.4/9149